scientific reports

Check for updates

OPEN

Method for label-free & non-destructive detection of microplastics in human formalin-fixed paraffin-embedded tissue sections

Elisabeth S. Gruber[1]✉, Verena Karl[2], Kristina Duswald[2,3], Mukund S. Bhamidipalli[2], Michaela Schlederer[4], Tanja Limberger[3], Verena Kopatz[4,5,9], Béla Teleky[6], Lukas Kenner[3,4,7,8,9,10,11]✉ & Markus Brandstetter[2,3,11]✉

Microplastic (MP) pollution is increasingly acknowledged as a critical environmental and public health issue. This study sought to establish a robust, clinically compatible method for detecting MP particles in deparaffinized formalin-fixed paraffin-embedded (FFPE) human colon tissue sections, using protocols compatible with routine clinical pathology. We employed mid-infrared photothermal (MIP) microscopy—also referred to as optical photothermal infrared (OPTIR) spectroscopy—as a non-destructive, high-resolution technique for chemical characterization and spatial mapping of polymer particles in intact FFPE samples. Following OPTIR analysis, identical sections underwent hematoxylin and eosin (H&E) staining to facilitate precise histopathological evaluation in defined regions of interest. Using this integrated workflow, we detected and localized polyethylene (PE), polystyrene (PS), and polyethylene terephthalate (PET) particles (21 PE particles, 1 PS particle, and 1 PET fiber) within distinct tissue areas. Subsequent histological assessment revealed characteristic inflammatory features near to these identified MP particles. To our knowledge, this represents the first demonstration of a diagnostic workflow that enables combined infrared spectroscopic and histopathological analysis of MPs in routinely processed human FFPE tissue. This approach offers a promising avenue to elucidate the role of microplastic accumulation in human disease and supports further investigation into potential mechanistic links between MP exposure and inflammatory processes in the colon.

Keywords Microplastic, FFPE, Colon, Inflammation, Optical photothermal infrared spectroscopy

Microplastics (MPs), defined as plastic particles smaller than five millimeters, have been identified across a broad spectrum of environmental compartments, including marine and freshwater systems, soil, and the atmosphere[1–4]. Their pervasive distribution has heightened concerns about potential implications for human health[5–7]. Emerging evidence suggests that diverse MP types can enter the human body through ingestion or inhalation and may accumulate within various organs[8–29].

Polyethylene (PE), polystyrene (PS), and polyethylene terephthalate (PET) are commonly used plastics for food and beverage packaging[30] and pose several potential threats to human health, particularly due to their

[1]Department of General Surgery, Medical University Vienna, Vienna, Austria. [2]Research Center for Non-Destructive Testing (RECENDT), Linz, Austria. [3]Center for Biomarker Research in Medicine (CBmed), Graz, Austria. [4]Clinical Institute of Pathology, Department of Experimental and Laboratory Animal Pathology, Medical University of Vienna, Vienna, Austria. [5]Department for Radiation Oncology, Medical University of Vienna, Vienna, Austria. [6]Center for Biomedical Research and Translational Surgery, Medical University of Vienna, Vienna, Austria. [7]Christian Doppler Laboratory for Applied Metabolomics, Medical University of Vienna, Vienna, Austria. [8]Unit of Laboratory Animal Pathology, University of Veterinary Medicine Vienna, Vienna, Austria. [9]Comprehensive Cancer Center, Medical University Vienna, Vienna, Austria. [10]Department of Molecular Biology, Umeå University, Umeå, Sweden. [11]Lukas Kenner and Markus Brandstetter jointly supervised this work. ✉email: elisabeth.s.gruber@meduniwien.ac.at; lukas.kenner@meduniwien.ac.at; markus.brandstetter@recendt.at

chemical composition and the way they are used or disposed of. While the risks vary depending on exposure levels and individual susceptibility[31], the potential health impacts of these plastics are significant, especially in contexts of prolonged or high-level exposure. They can release harmful chemicals, especially when heated or degraded. PS can leach styrene, a possible carcinogen that may cause nervous system effects, irritation, and other health issues[32,33]. PE, though generally considered safer, can release additives or byproducts during manufacturing or when exposed to heat[34]. As PE and PS degrade, they break down into MP particles, which can be ingested through food, water, and air, leading to potential health risks such as inflammation, oxidative stress, and disruption of cellular processes[35–38]. Further (indirect) health impacts can occur through accumulation of PE and PS in the environment, particularly in oceans, contaminating food sources, such as particularly seafood, introducing toxins into the food chain. Generally regarded as safe for food contact[30], PET raises concerns when degraded into MP particles entering the human body[22,24]. Studies suggest that PET can carry harmful chemicals like antimony[39,40]. While there is no conclusive evidence of serious health effects from PET exposure in typical use, the potential for chemical leaching and long-term health risks remains a topic of ongoing research.

Despite growing concerns about the potential health risks of such MP particles, studying their direct effects on the human body remains a challenge. In particular, it is difficult to detect and localize MP particles in human tissue taken as part of routine medical examinations, such as it is the case for formalin-fixed paraffin-embedded tissue (FFPE) used for histopathological analysis and reporting. The tiny size of the particles, their chemical composition and the limited sensitivity of current analytical methods make detection – without losing information about the exact position – difficult, further complicating research into their long-term health effects.

Infrared spectroscopy is a widely used label-free and non-destructive technique to obtain qualitative and quantitative information of organic and inorganic samples. The mid-infrared (MIR) part of the infrared spectrum is here of particular interest as it provides a (bio-)chemical fingerprint and therefore allows characterization and discrimination of biological structures such as lipids, DNA and proteins, e.g., to distinguish diseased from healthy sections[41,42]. Furthermore, MIR spectroscopy can be used to detect and identify (M)P particles due to their unique chemical compositions. Due to technological limitations of established MIR spectroscopy methods, the current standard procedure for that kind of analysis involves the chemical or enzymatic digestion of the entire tissue sample to remove any biological components. After filtration of the solution, the remaining (M)P particles are collected on a suitable filter for spectroscopic characterization[8–17,19–29]. However, tissue digestion results in the complete loss of tissue architecture and hence spatial information of accumulated (M)P particles. However, for deeper clinical insight on uptake and accumulation of MPs, it is crucial to identify the precise spatial particle distribution in the respective tissues. To meet this urgent technical need, the recently introduced optical photothermal infrared (OPTIR) spectroscopy technique was employed on deparaffinized human colon samples. OPTIR spectroscopy is characterized by a series of advances compared to conventional MIR spectroscopy methods, among them a significantly improved lateral resolution (~ 500 nm) beyond the classical infrared diffraction limit, the ability to measure in reflection geometry on standard glass sample carriers and the absence of spectral artifacts, which are particularly challenging when small structures are investigated[43].

The primary objective of this study was to develop and validate a robust method for detecting microplastic (MP) particles in formalin-fixed paraffin-embedded (FFPE) human colon tissue sections, using polyethylene (PE), polystyrene (PS), and polyethylene terephthalate (PET) as representative target polymers commonly associated with food and beverage packaging[30]. To inform spectroscopic analysis, haematoxylin and eosin (H&E)-stained sections were evaluated in a blinded manner. Regions of interest were defined based on established criteria[44], allowing for targeted, high-resolution, and label-free detection of MPs using optical photothermal infrared (OPTIR) spectroscopy. Specific methodological objectives included the refinement of tissue preparation protocols and the application of OPTIR for precise chemical characterization and spatial localization of MPs within intact histological sections.

Materials and methods

Sample collection and preparation

The three FFPE colon tissue samples used in this study were obtained from routine surgical resections performed for inflammatory, non-neoplastic indications. Tissue blocks were selected from morphologically unremarkable areas, distant from any pathological lesions. Samples underwent standard paraffinization work-up to ensure routine histopathological examination and reporting. For this, the samples were fixed in 10% formalin for 24–48 h. Following fixation, the tissues were dehydrated through a graded series of ethanol solutions, cleared in xylene, and embedded in paraffin blocks. Ethical approval for the study was obtained from the institutional review board ('Ethikkommission' of the Medical University of Vienna, protocol no. 1003/2024) and informed consent was waived off. All methods were carried out in accordance with relevant guidelines and regulations.

For MP analysis, sections of 5 µm thickness were cut from paraffin blocks using a microtome and mounted on both standard glass (for OPTIR analysis) and low-e (for laser direct infrared (LDIR) imaging analysis) microscope slides. To limit signal reduction and hence spectral characteristics of tissue samples[45], deparaffinization was performed according to an established protocol[46]: In short, slides were first heated to melt the paraffin. After rehydration through graded isopropyl alcohol solutions, the slides were first analysed with infrared spectroscopy (OPTIR and/or LDIR) and then stained with hematoxylin and eosin (H&E staining). Partial dehydration was done before eosin application, and the slides were mounted with aqueous glycerol and sealed with nail polish.

Optical photothermal infrared (OPTIR) spectroscopy

For the acquisition of infrared spectra an OPTIR system (mIRage + R, Photothermal Spectroscopy Corp., USA) was employed. The OPTIR technique utilizes a pump-probe approach where the material-dependent spectral absorption of a mid-infrared laser induces a photothermal effect that is read out by a visible laser. The system uses a widely tunable MIR quantum cascade laser (QCL) to locally excite a sample. When the sample absorbs a

photon of a specific MIR wavelength, different photothermal effects are triggered (expansion, refractive index change). A second readout laser (532 nm) then probes the photothermal effects, allowing for the detection of the smallest changes[47]. Selectivity is obtained by the wavelength selective measurement, whereas sensitivity is obtained by the signal strength, which correlates with the amount of substance present. This approach overcomes the infrared diffraction limit and achieves a spatial resolution improved by a factor of ~ 30 when compared to conventional FTIR microscopes[48]. Thus, small structures such as MP particles embedded in complex tissues can be resolved in the submicron range (~ 500 nm). For selected samples, additional large-area overview scans at standard infrared resolution limits using laser direct infrared (LDIR) imaging were performed (8700 LDIR Chemical Imaging System, Agilent Technologies, USA). The purpose of these measurements was a faster recognition of larger MP structures (e.g., polymer fibers). Both OPTIR and LDIR were tailored precisely for application to deparaffinized sections.

Workflow for Spatial localization and chemical identification of microplastic particles

To allow for a clear spatial identification of MP particles, an optimized spectroscopic workflow was elaborated by exemplarily focusing on PE particles (Fig. 1). The visible image shows the standard optical microscope image of the sample. The chemical images "tissue" and "PE" are derived from the measured infrared absorption at specific wavelengths that are known to be characteristic for tissue and PE, respectively. In this study, the presence of tissue is visualized by generating chemical images derived from the intensity of the amide I band (1660 cm^{-1}), as it is a characteristic marker for proteins and organic tissue. In contrast, chemical imaging for the detection of MPs is conducted at a polymer specific wavelength (e.g., represented by the C-H stretching vibration of PE at 2855 cm^{-1}). The final step of image processing is illustrated in the chemical image "PE/tissue", where the ratio of the chemical image intensities of PE and tissue is calculated. The effect of this approach can be interpreted as background normalization. While distinct structures are not recognizable in the single chemical images, the here conducted ratio calculation effectively highlights three PE particles. As demonstrated in subsequent figures, this technique is well suited to distinctly differentiate polymer structures from the surrounding tissue, based on the spectral information obtained at characteristic wavenumbers (= inverse wavelength).

After implementing these technical optimizations, the following "optimized" workflow was defined for the detection of MP particles:

1. Acquisition of visible images of the entire tissue section using the internal optical microscope of the OPTIR system.
2. Selection of distinct regions of interest (region I - mucosa, region II - muscularis, region III - serosa) in the respective colon tissue sections (Fig. 2).
3. Chemical Analysis of each region and identification of suspicious particles based on a 2D image recorded at characteristic wavenumbers targeting the polymer type of interest.
4. Validation of the identified PE, PS and/or PET particles based on their characteristic spectral fingerprint (unveiling the chemical nature of the distinct particles by recording full spectra).

The acquisition time for such a chemical image is strongly influenced by the desired spatial resolution and the total number of pixels. It can vary substantially depending on the chosen measurement parameters. As an illustrative example, acquiring an image with dimensions of 100 × 100 pixels with a step size of 0.1 µm requires

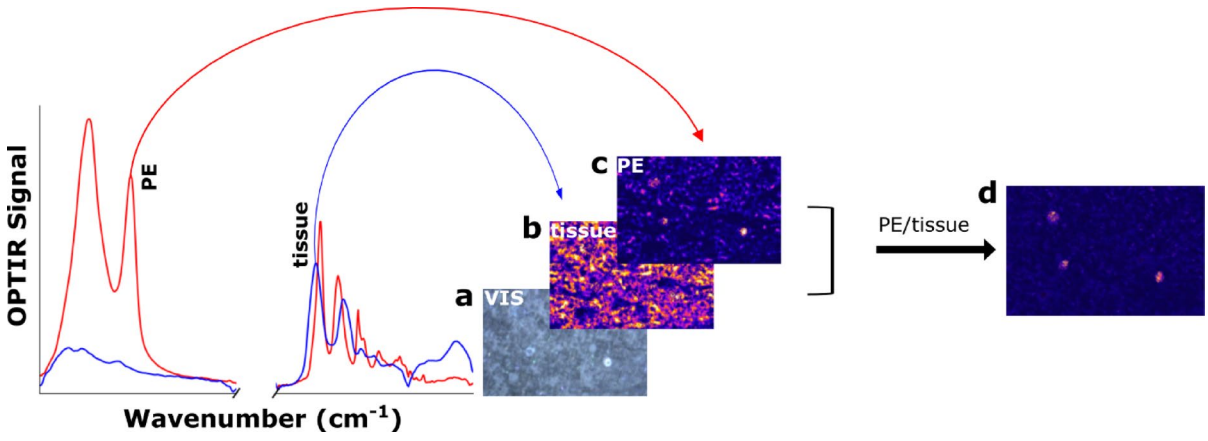

Fig. 1. Elaboration of a spectroscopic workflow for optimized MP particle detection. (**a**) The visible image (VIS) represents the standard optical microscope image of unstained tissue; (**b**) The "tissue"-image shows a chemical image (wavenumber 1660 cm^{-1}); (**c**) the "PE"-image shows a chemical image (wavenumber 2855 cm^{-1}) characteristic for the polymer of interest (here: PE). (**d**) Final step: "PE/tissue"-image, calculated as the ratio of "PE"- and "tissue"-image, resulting in a clear identification of PE particles at three different positions within the section/region of interest.

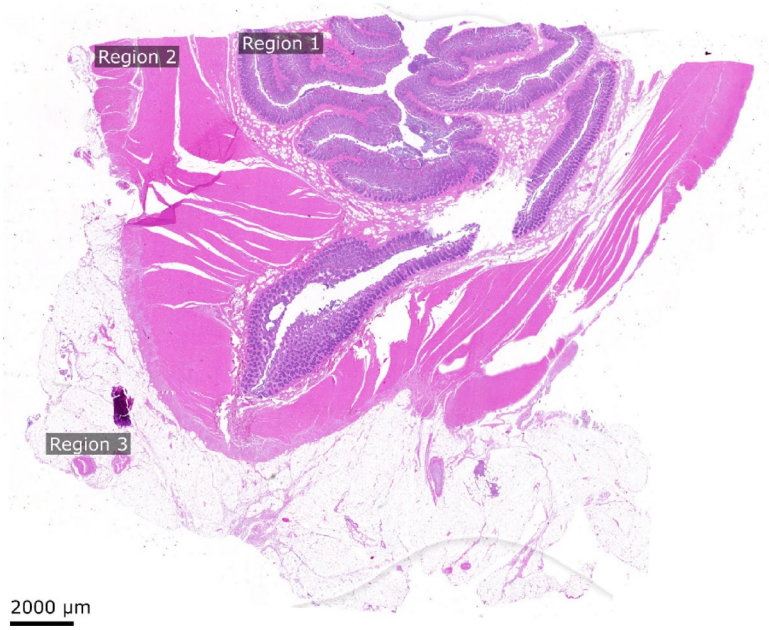

Fig. 2. Regions of interest for the exact spatial localization of MP particles. Three regions were defined: region I – mucosa, region II – muscularis and region III – serosa. Since particles are suspected to be absorbed via the mucosa, the primary focus was set to region I and II, which were then analogously inspected for suspicious particles.

approximately 45 s. Of note, this workflow is highly versatile and can be adapted to detect any polymer type by simply modifying the selected target wavenumbers in step 3.

Histopathological analysis

Histological evaluation was conducted on hematoxylin and eosin (H&E)-stained colon sections to delineate regions of interest for subsequent optical photothermal infrared (OPTIR) analysis. Evaluation was carried out by L.K., a board-certified pathologist with over 20 years of experience in human pathology, including gastrointestinal diseases. All evaluations were performed in a blinded manner following standardized criteria adapted from Crnčec et al.[44]. Histological parameters, including the extent of inflammatory cell infiltration, alterations in crypt architecture alterations, and the presence of ulcerations were examined. Regions exhibiting prominent histopathological changes—such as increased inflammatory infiltrates, crypt damage, or mucosal erosion—were identified and designated as regions of interest. These predefined areas subsequently guided OPTIR spectroscopy measurements, enabling precise spatial correlation between morphological tissue alterations and the presence of microplastic particles. All evaluations were performed under uniform staining conditions and representative areas were selected to minimize sampling bias.

Results

Three human colon sections (sample 1, sample 2 and sample 3) were analysed individually in this study using the optimized workflow described in the experimental section. This approach facilitated the unambiguous identification of MP particles in deparaffinized clinical routine samples. In this section, we validate these reported findings through chemical imaging at characteristic wavenumbers and acquisition of full spectral data. Additionally, we examine the potential influence of residual paraffin on the results and provide an exemplary region from sample 1 (H&E-stained), demonstrating signs of inflammation in close proximity to MP particles.

Using the established OPTIR workflow, three different types of microplastic particles—polyethylene (PE), polystyrene (PS), and polyethylene terephthalate (PET)—were detected in FFPE colon tissue sections. In sample 1, a total of 21 predominantly spherical PE particles (approximately 3–6 µm in size) were identified in two distinct regions: 13 in region I and 8 in region II. In sample 2, a single PS particle was detected, and in sample 3, one PET fibre was identified. The spectroscopic profiles of all particles showed high concordance with corresponding reference spectra, confirming their chemical identity.

Impact of paraffin residues on spectral analysis

Clinical tissue samples are typically embedded in FFPE blocks to ensure long-term preservation. As part of the standard workflow, sample deparaffinization is performed prior to further analyses. This step is also critical for OPTIR measurements, as paraffin or polyisobutylene can substantially attenuate signals from underlying substances, significantly obscuring the spectral characteristics of the embedded tissue . Residual paraffin or polyisobutylene remaining sample preparation[49,50] may interfere with MP particle identification within tissue sections. Figure 3 illustrates how minor residues of paraffin and polyisobutylene persist on the sample slide

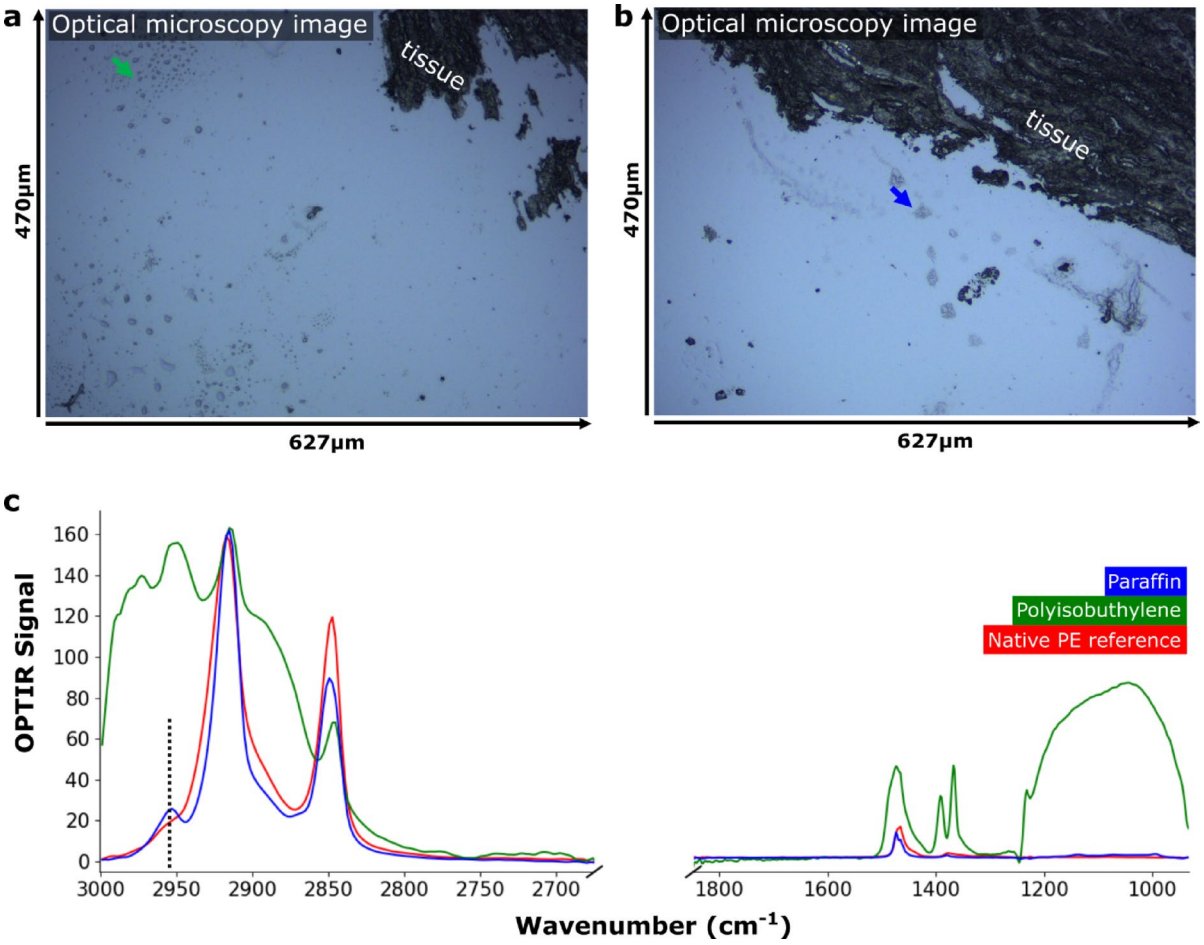

Fig. 3. Example of material residues on a tissue slide after deparaffinization and discrimination from MP particles by exploiting characteristic spectral features. Residues of (**a**) polyisobutylene (green arrow) and (**b**) paraffin (blue arrow) that challenge the identification of MP particles. (**c**) One specific band, centered at wavenumber 2959 cm^{-1} can be used to clearly discriminate paraffin and PE, a common MP polymer. In contrast, polyisobutylene exhibits a spectral signature that can be clearly differentiated from that of paraffin, indicating that the presence of polyisobutylene does not interfere with the detection of PE.

adjacent to the tissue sections. In particular, the spectral discrimination between PE and paraffin is challenging, given that their infrared spectra exhibit only subtle differences compared to other polymer types. Nevertheless, the band at 2959 cm, indicated by a dashed line in Fig. 3c, ultimately enabled clear differentiation between the different PE and paraffin.

Identification and localization of polyethylene (PE) and polystyrene (PS) particles

Figure 4a exemplifies the detection and identification of PE particles in region II of sample 1. As demonstrated, we achieved precise localization of MP particles within organic tissue using single-wavelength scans. For validation, full spectral analysis of the detected particles confirmed the characteristic chemical fingerprint of PE and delineated the amide I and amide II bands indicative of tissue. Notably, both amide bands exhibited a spectral shift relative to the adjacent tissue (amide I from 1660 cm^{-1} to 1645 cm^{-1} and amide II from 1545 cm^{-1} to 1563 cm^{-1}), suggesting potential PE-tissue interactions or alterations. To further substantiate the identification of the plastic type as PE, we performed a detailed comparison of signal intensities in the C-H fingerprint region: discrimination of PE from polyamide was achieved by demonstrating significantly higher intensities for PE (2853 cm^{-1} and 2923 cm^{-1}) compared to polyamide (2861 cm^{-1} and 2929 cm^{-1})[51].

Figure 4b highlights the observation of an isolated PS particle (approximately 10 µm in size), detected in region I of sample 2. The differences between the ratio plots for PS and PE (Fig. 4b) are less pronounced than those used to validate PE particles (Fig. 4a). This is attributed to the non-zero absorption of PS at 2855 cm^{-1} (visible in the plotted PS spectrum), which contributes to signals appearing in the PE ratio, as the wavenumber 2855 cm^{-1} is employed in this ratio plot. However, PS can be distinctly identified via direct comparison of the calculated ratio plots. This example clearly illustrates a limitation of pure ratio plots, thus full spectral analysis of the sample of interest is recommended to obtain comprehensive chemical information. Detailed analysis of the individual PS MP particle further revealed well-defined amide bands without any spectral shift (amide I

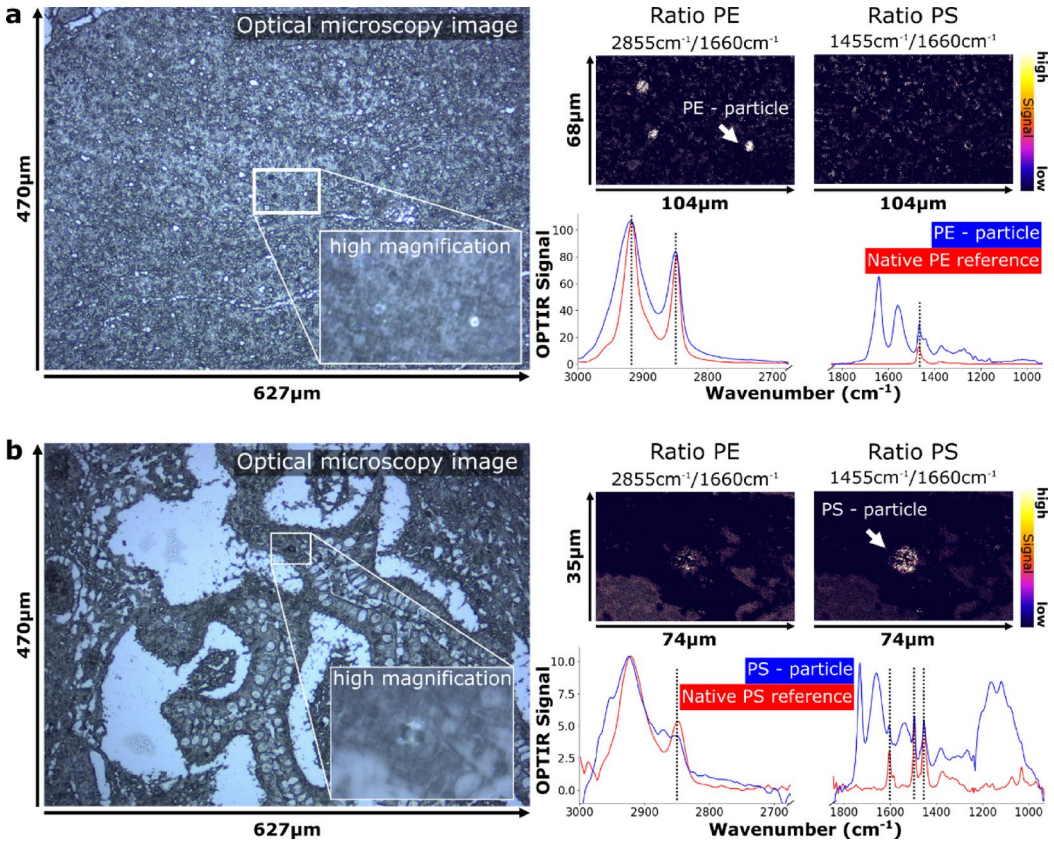

Fig. 4. Representative detection and validation of polyethylene (PE), and polystyrene (PS) particles in FFPE human colon tissue using OPTIR spectroscopy. (**a**) Visible image of region II (muscularis) in sample 1 showing the area where PE particles (~ 4 µm) are identified. Bright spots are observed in the corresponding chemical ratio image for PE (wavenumber ratio 2855/1660 cm^{-1}), whereas the ratio image for PS (wavenumber ratio 1455/1660 cm^{-1}) serves as a negative control; subsequent full spectral analysis at the detected points revealed a strong correlation with the characteristic PE bands, observed at wavenumbers 2923 cm^{-1}, 2855 cm^{-1} and 1467 cm^{-1} of a native PE reference sample. (**b**) Analysis of region I (mucosa) of sample 2, similar to Fig. 4a. Identification of a single PS particle using vibrational bands indicative for PS (correlation with native sample spectrum at characteristic wavenumbers 1602 cm^{-1}, 1495 cm^{-1} and 1455 cm^{-1}) and amide (notably at 1660 cm^{-1} and 1545 cm^{-1}), supporting the particle's localization within biological tissue. The spectral signature shown here for PE and PS particles, mixed with characteristic amide bands confirm the presence of embedded plastic material.

band at 1660 cm^{-1}, amide II band at 1545 cm^{-1}). However, a significant difference was observed in the form of a prominent band at 1735 cm^{-1}, which is not present in the reference spectrum of native PS. Consequently, this band may originate from chemical modification of the particle, or alternatively, it may reflect the presence of lipids adsorbed onto the particle.

Identification and localization of a polyethylene terephthalate (PET) fiber

Figure 5 illustrates a PET-based fiber (approximately 1000 µm x 13 µm) identified within region I of sample 3. The ratio plot indicative of PET clearly delineates the position of the detected fiber and demonstrates embedding within the tissue matrix. Upon closer examination using the high-resolution chemical image in Fig. 5b, variations in signal intensities are observed at multiple locations along the fiber. Full spectral analysis of these specific regions revealed partial incorporation of the fiber into the surrounding tissue matrix[52], as evidenced by the presence of the characteristic signals for both PET and tissue within the recorded spectra at these respective locations.

Inflammatory lesions in colon tissue detected by H&E staining

We investigated potential correlations between the presence of microplastic particles and histopathological signs of inflammation. The H&E-stained tissue sections revealed the spatial distribution of MPs in close association with characteristic inflammatory features (Fig. 6). In particular, MPs were localized near focal, patchy lesions, characterized by lymphocytic infiltration selectively affecting certain regions while sparing others, resembling patterns seen in colitis. In addition, MPs were identified in regions exhibiting thickening of the muscularis propria, where we also noted significant neural hyperplasia, characterized by an increased number and size of nerve bundles. These features - patchy chronic inflammation, transmural thickening, and neural hyperplasia

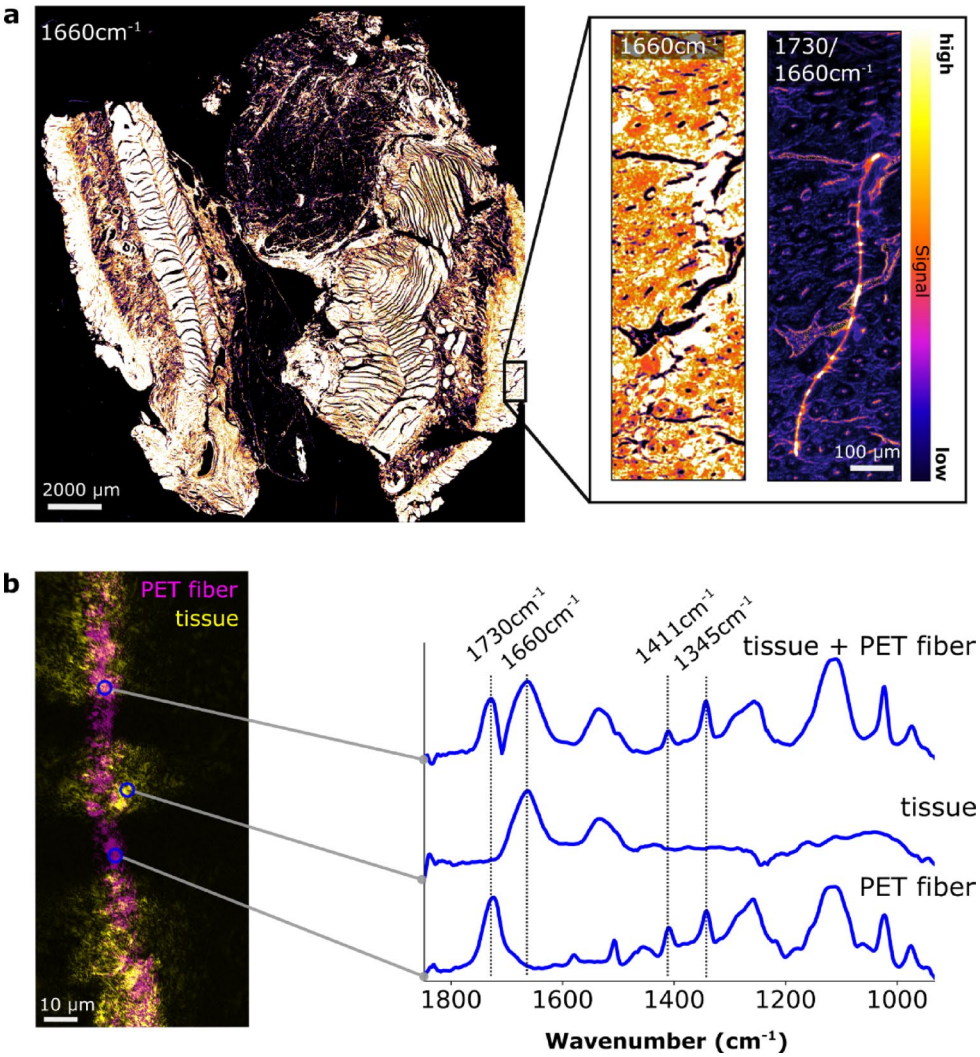

Fig. 5. Representative detection and validation of polyethylene terephthalate (PET) fiber-based fragment in FFPE human colon tissue using LDIR and OPTIR spectroscopy. (**a**) Chemical image (recorded at wavenumber 1660 cm^{-1}) of sample 3 provides an overview of the entire cross-section (LDIR, 3 µm resolution). Subsequent chemical imaging of a defined area with higher spatial resolution (LDIR, 1 µm resolution) results in a clear visualization of the fiber. The calculated ratio image (wavenumber 1730/1660 cm^{-1}) strongly indicates that the PET fiber is embedded within the tissue matrix. (**b**) The chemical image overlay (1660 cm^{-1} and 1730 cm^{-1}) reveals the distinct spatial distribution of the fiber, tissue material, and areas where the fiber is fully embedded. Full spectral analysis at each point is presented in the spectral fingerprint region (OPTIR, 500 nm resolution).

observed in the proximity to MPs - may suggest a potential association between MP exposure and colonic inflammatory processes.

Discussion

According to the documented accumulation of MP particles in human tissues[8–29], the need for research into their potential health risks is of paramount importance. OPTIR, a novel non-contact spectroscopic technique, is particularly well suited for chemical imaging of soft tissues. This non-destructive method preserves tissue architecture, enabling subsequent histopathological analyses critical for understanding the clinical impact of MP accumulation, without the need for specialized substrates or sample preparation, maintaining standardized protocols already well integrated into clinical workflows. For more robust analyses, an automated method for quantitative particle assessment remains to be developed. As demonstrated in the recorded infrared spectra, this approach is also influenced by the chemical composition of the surrounding tissue. By contrast, methods involving tissue digestion[8–17,19–29] eliminate this effect yield clearer polymer spectra. The strong presence of amide bands I and II, indicative of biological components, results in a mixed spectrum of tissue and polymer, complicating precise chemical identification. Furthermore, alterations in the polymer composition induced by environmental exposure or chemical agents used for tissue fixation represent critical factors in the identification process. Polymer degradation may lead to the emergence of new spectral peaks, peak shifts, or the loss of

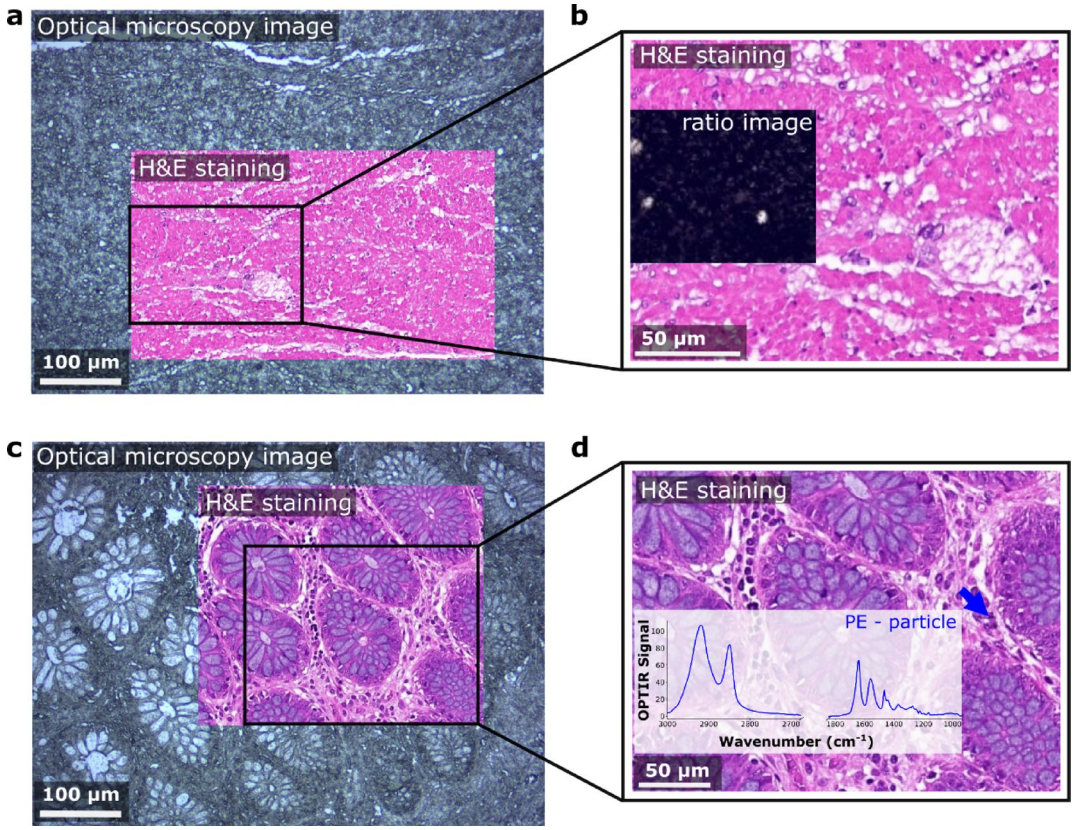

Fig. 6. H&E analysis. (**a**). Optical image of sample 1 in region II (muscularis) and a partial overlay with the corresponding H&E image. (**b**) Magnified view of the H&E stained region where PE particles were found and verified via chemical image analysis. (**c**) Optical image of sample 1 in region I (mucosa) and a partial overlay with the corresponding H&E image. (**d**) Depicts a magnified view of the H&E stained region; an isolated PE particle found in that region and verified by chemical analysis is indicated with a blue arrow. The corresponding spectrum of this particle is shown as inset.

characteristic signals. Given that the tissue sections investigated are untreated samples, no information is available regarding the origin or age of these particles, which may account for minor spectral variations observed relative to reference spectra.

Our results demonstrate a significant association between the presence of MPs and characteristic histopathological features of colitis. These histomorphologic alterations suggest that MPs may contribute to the induction of inflammatory processes.

This study is limited by the small number of analysed samples ($n=3$), which constrains the ability to generalize the findings. However, as a proof-of-concept investigation, the primary goal was to demonstrate the feasibility of applying OPTIR spectroscopy to routinely processed FFPE human tissues for the detection and spatial localization of microplastics (MPs). The methodological robustness and compatibility with existing histopathological workflows highlight the potential of this approach for broader clinical and translational applications. In particular, the ability to retrospectively screen archived clinical material may enable future large-scale investigations into MP accumulation in human tissues, supporting epidemiological studies and informing regulatory discussions on exposure risks. Validation in larger and more diverse patient cohorts will be essential to assess diagnostic sensitivity, clinical significance, and possible associations with chronic inflammatory or neoplastic diseases.

While the present study primarily focused on demonstrating the feasibility of MP detection and spatial localization using OPTIR spectroscopy, future developments should aim to enable systematic and quantitative assessments of microplastic burden in human tissues. Automated image analysis, supported by advances in digital pathology, could facilitate reproducible particle detection across large datasets. In particular, machine learning-based segmentation and classification tools offer the potential to standardize MP identification, reduce observer bias, and improve throughput. Integration of such algorithms with spectroscopic and histological data would support the development of quantitative metrics for MP exposure at the tissue level, enabling more robust comparisons across individuals, tissue types, and disease states. To ensure reproducibility and translational relevance, future work should also focus on validating these approaches across laboratories and establishing consensus standards for MP quantification in biological tissues.

Given its compatibility with standard FFPE tissue processing, the presented workflow could be readily applied to other organ systems and clinical conditions potentially affected by MP exposure. This includes tissues

from the respiratory, gastrointestinal, or reproductive tract, where environmental contaminants may contribute to chronic inflammation or disease progression. Importantly, the method enables retrospective analyses of archived pathology specimens, offering a scalable approach for investigating MP burden across large patient cohorts. The feasibility of such large-scale screening is supported by recent advances in digital pathology and biobank accessibility[53], which may facilitate the integration of environmental exposure data into clinical research and risk assessment frameworks.

Summary and conclusion

This study demonstrates the detection and identification of MP particles in routinely processed FFPE human colon tissue sections. To our knowledge, this is the first report of MP identification within this clinical context. By employing optical photothermal infrared (OPTIR) spectroscopy, we achieved submicron spatial resolution, enabling precise localization and chemical identification of PE, PS and PET particles, surpassing the spatial limitations of conventional infrared microscopy. We describe the integration of spectroscopic and histopathological analyses within a single diagnostic workflow, which may provide valuable insights into MP accumulation in human tissues. The spatial association of MPs with inflammatory histological features supports the hypothesis of a potential link between MP exposure and colonic inflammation. These findings lay the groundwork for further investigations into the role of MPs in gastrointestinal and other inflammatory diseases.

Data availability

The datasets generated and/or analyzed during the current study are available from the corresponding author on reasonable request.

Received: 29 July 2025; Accepted: 30 October 2025
Published online: 28 November 2025

References

1. Boccia, P. et al. Potential effects of environmental and occupational exposure to microplastics: an overview of air contamination. *Toxics* **12** https://doi.org/10.3390/toxics12050320 (2024).
2. Communication, T. E. P.-D. G. f. Microplastics: sources, effects and solutions. (2018).
3. Maurizi, L., Simon-Sánchez, L., Vianello, A., Nielsen, A. H. & Vollertsen, J. Every breath you take: high concentration of breathable microplastics in indoor environments. *Chemosphere* **361**, 142553. https://doi.org/10.1016/j.chemosphere.2024.142553 (2024).
4. Tang, L. et al. Global occurrence, drivers, and environmental risks of microplastics in marine environments. *J. Environ. Manage.* **329**, 116961. https://doi.org/10.1016/j.jenvman.2022.116961 (2023).
5. Borgatta, M. & Breider, F. Inhalation of Microplastics-A toxicological complexity. *Toxics* **12** https://doi.org/10.3390/toxics12050358 (2024).
6. Gruber, E. S. et al. To waste or not to waste: questioning potential health risks of Micro- and nanoplastics with a focus on their ingestion and potential carcinogenicity. *Expo Health*. **15**, 33–51. https://doi.org/10.1007/s12403-022-00470-8 (2023).
7. Wright, S. L. & Kelly, F. J. Plastic and human health: A micro issue? *Environ. Sci. Technol.* **51**, 6634–6647. https://doi.org/10.1021/acs.est.7b00423 (2017).
8. Amato-Lourenço, L. F. et al. Presence of airborne microplastics in human lung tissue. *J. Hazard. Mater.* **416**, 126124. https://doi.org/10.1016/j.jhazmat.2021.126124 (2021).
9. Braun, T. et al. Detection of microplastic in human placenta and meconium in a clinical setting. *Pharmaceutics* **13** https://doi.org/10.3390/pharmaceutics13070921 (2021).
10. Garcia, M. A. et al. Quantitation and identification of microplastics accumulation in human placental specimens using pyrolysis gas chromatography mass spectrometry. *Toxicol. Sci.* **199**, 81–88. https://doi.org/10.1093/toxsci/kfae021 (2024).
11. Guo, X. et al. Discovery and analysis of microplastics in human bone marrow. *J. Hazard. Mater.* **477**, 135266. https://doi.org/10.1016/j.jhazmat.2024.135266 (2024).
12. Horvatits, T. et al. Microplastics detected in cirrhotic liver tissue. *EBioMedicine* **82**, 104147. https://doi.org/10.1016/j.ebiom.2022.104147 (2022).
13. Huang, S. et al. Detection and analysis of microplastics in human sputum. *Environ. Sci. Technol.* **56**, 2476–2486. https://doi.org/10.1021/acs.est.1c03859 (2022).
14. Ibrahim, Y. S. et al. Detection of microplastics in human colectomy specimens. *JGH Open.* **5**, 116–121. https://doi.org/10.1002/jgh3.12457 (2021).
15. Jenner, L. C. et al. Detection of microplastics in human lung tissue using μFTIR spectroscopy. *Sci. Total Environ.* **831**, 154907. https://doi.org/10.1016/j.scitotenv.2022.154907 (2022).
16. Leslie, H. A. et al. Discovery and quantification of plastic particle pollution in human blood. *Environ. Int.* **163**, 107199. https://doi.org/10.1016/j.envint.2022.107199 (2022).
17. Liu, S. et al. Detection of various microplastics in placentas, meconium, infant feces, breastmilk and infant formula: A pilot prospective study. *Sci. Total Environ.* **854**, 158699. https://doi.org/10.1016/j.scitotenv.2022.158699 (2023).
18. Min, H. J., Kim, K. S., Kim, H., Gong, J. & Jeong, J. Identification and characterization of microplastics in human nasal samples. *Int. Forum Allergy Rhinol.*. https://doi.org/10.1002/alr.23427 (2024).
19. Montano, L. et al. Raman microspectroscopy evidence of microplastics in human semen. *Sci. Total Environ.* **901**, 165922. https://doi.org/10.1016/j.scitotenv.2023.165922 (2023).
20. Pironti, C. et al. First Evidence of Microplastics in Human Urine, a Preliminary Study of Intake in the Human Body. *Toxics* 11, https://doi.org/10.3390/toxics11010040 (2022).
21. Ragusa, A. et al. Raman microspectroscopy detection and characterisation of microplastics in human breastmilk. *Polym. (Basel).* 14. https://doi.org/10.3390/polym14132700 (2022).
22. Ragusa, A. et al. First evidence of microplastics in human placenta. *Environ. Int.* **146**, 106274. https://doi.org/10.1016/j.envint.2020.106274 (2021). Plasticenta.
23. Rotchell, J. M. et al. Detection of microplastics in human saphenous vein tissue using μFTIR: A pilot study. *PLoS One.* **18**, e0280594. https://doi.org/10.1371/journal.pone.0280594 (2023).
24. Schwabl, P. et al. Detection of various microplastics in human stool. *Ann. Intern. Med.* **171**, 453–457. https://doi.org/10.7326/M19-0618 (2019).
25. Wu, D. et al. Pigment microparticles and microplastics found in human thrombi based on Raman spectral evidence. *J. Adv. Res.* **49**, 141–150. https://doi.org/10.1016/j.jare.2022.09.004 (2023).

26. Yang, Y. et al. Detection of various microplastics in patients undergoing cardiac surgery. *Environ. Sci. Technol.* **57**, 10911–10918. https://doi.org/10.1021/acs.est.2c07179 (2023).
27. Yun, X. et al. Raman-guided exploration of placental microplastic exposure: unraveling the polymeric tapestry and assessing developmental implications. *J. Hazard. Mater.* **477**, 135271. https://doi.org/10.1016/j.jhazmat.2024.135271 (2024).
28. Zhao, Q. et al. Detection and characterization of microplastics in the human testis and semen. *Sci. Total Environ.* **877**, 162713. https://doi.org/10.1016/j.scitotenv.2023.162713 (2023).
29. Zhu, L. et al. Identification of microplastics in human placenta using laser direct infrared spectroscopy. *Sci. Total Environ.* **856**, 159060. https://doi.org/10.1016/j.scitotenv.2022.159060 (2023).
30. ACC. American Chemistry Council, (2024).
31. BfR. *Mikroplastik: Fakten, Forschung und offene Fragen*, https://www.bfr.bund.de/de/mikroplastik__fakten__forschung_und_offene_fragen-192185.html (2024).
32. WHO, W. H. O. Chemical fact sheets: Styrene. 465–466 (Water, Sanitation, Hygiene and Health (WSH). (2022).
33. Kogevinas, M. et al. Carcinogenicity of quinoline, styrene, and styrene-7,8-oxide. *Lancet Oncol.* **19**, 728–729. https://doi.org/10.1016/S1470-2045(18)30316-4 (2018).
34. Ronca, S. in *Brydson's Plastics Materials (Eighth Edition)* (ed Marianne Gilbert) 247–278 (Butterworth-Heinemann, (2017).
35. Ghosal, S., Bag, S., Rao, S. R. & Bhowmik, S. Exposure to polyethylene microplastics exacerbate inflammatory bowel disease tightly associated with intestinal gut microflora. *RSC Adv.* **14**, 25130–25148. https://doi.org/10.1039/d4ra04544k (2024).
36. Hameister, R., Kaur, C., Dheen, S. T., Lohmann, C. H. & Singh, G. Reactive oxygen/nitrogen species (ROS/RNS) and oxidative stress in arthroplasty. *J. Biomed. Mater. Res. B Appl. Biomater.* **108**, 2073–2087. https://doi.org/10.1002/jbm.b.34546 (2020).
37. Wu, H., Guo, J., Yao, Y. & Xu, S. Polystyrene nanoplastics induced cardiomyocyte apoptosis and myocardial inflammation in carp by promoting ROS production. *Fish. Shellfish Immunol.* **125**, 1–8. https://doi.org/10.1016/j.fsi.2022.04.048 (2022).
38. Xiang, W. & Chen, L. In light-sensitive drug delivery system nanoparticles mediate oxidative stress. *Am. J. Transl Res.* **12**, 1469–1480 (2020).
39. Allafi, A. R. The effect of temperature and storage time on the migration of antimony from polyethylene terephthalate (PET) into commercial bottled water in Kuwait. *Acta Biomed.* **91**, e2020105. https://doi.org/10.23750/abm.v91i4.8463 (2020).
40. Filella, M. Antimony and PET bottles: checking facts. *Chemosphere* **261**, 127732. https://doi.org/10.1016/j.chemosphere.2020.127732 (2020).
41. Colagar, A. H., Chaichi, M. J. & Khadjvand, T. Fourier transform infrared microspectroscopy as a diagnostic tool for distinguishing between normal and malignant human gastric tissue. *J. Biosci.* **36**, 669–677. https://doi.org/10.1007/s12038-011-9090-5 (2011).
42. Ramesh, J. et al. FTIR microscopic studies on normal and H-ras oncogene transfected cultured mouse fibroblasts. *Eur. Biophys. J.* **30**, 250–255. https://doi.org/10.1007/s002490100137 (2001).
43. Reffner, J. A. Advances in infrared microspectroscopy and mapping molecular chemical composition at submicrometer Spatial resolution. *Spectroscopy* **33** (9), 12–17 (2018).
44. Crnčec, I. et al. STAT1 is a sex-specific tumor suppressor in colitis-associated colorectal cancer. *Mol. Oncol.* **12**, 514–528. https://doi.org/10.1002/1878-0261.12178 (2018).
45. Hughes, C., Gaunt, L., Brown, M., Clarke, N. W. & Gardner, P. Assessment of paraffin removal from prostate FFPE sections using transmission mode FTIR-FPA imaging. *Anal. Methods.* **6**, 1028–1035. https://doi.org/10.1039/C3AY41308J (2014).
46. Gonçalves, C., Martins, M., Costa, M. H. & Costa, P. M. Development of a method for the detection of polystyrene microplastics in paraffin-embedded histological sections. *Histochem. Cell Biol.* **149**, 187–191. https://doi.org/10.1007/s00418-017-1613-1 (2018).
47. Baden, N., Kobayashi, H. & Urayama, N. Submicron-resolution polymer orientation mapping by optical photothermal infrared spectroscopy. *Int. J. Polym. Anal. Charact.* **25**, 1–7. https://doi.org/10.1080/1023666X.2020.1735851 (2020).
48. Kansiz, M. et al. Optical photothermal infrared microspectroscopy with simultaneous Raman - A new Non-Contact failure analysis technique for identification of < 10 Mum organic contamination in the hard drive and other electronics industries. *Micros Today.* **28**, 26–36. https://doi.org/10.1017/s1551929520000917 (2020).
49. Gaifulina, R. et al. Rapid and complete paraffin removal from human tissue sections delivers enhanced Raman spectroscopic and histopathological analysis. *Analyst* **145**, 1499–1510. https://doi.org/10.1039/C9AN01030K (2020).
50. Nallala, J., Lloyd, G. R. & Stone, N. Evaluation of different tissue de-paraffinization procedures for infrared spectral imaging. *Analyst* **140**, 2369–2375. https://doi.org/10.1039/c4an02122c (2015).
51. Prater, C. B., Kansiz, M. & Cheng, J. X. A tutorial on optical photothermal infrared (O-PTIR) microscopy. *APL Photonics*. **9**, 091101. https://doi.org/10.1063/5.0219983 (2024).
52. Bhamidipalli, M. S. *Spectroscopic Analysis of Microplastics: Overcoming Challenges in Complex Matrices* MSc thesis, FH Technikum Wien, (2024).
53. Eccher, A. et al. Automate the process of formalin-fixed paraffin-embedded blocks storage in the pathology laboratory: A proof of concept study. *Pathol. Res. Pract.* **266**, 155802. https://doi.org/10.1016/j.prp.2024.155802 (2025).

Author contributions

Conceptualization: E.S.G., T.L., L.K.; methodology: E.S.G., V.K., D.K., T.L., V.K., L.K., M.B.; software: not applicable; validation: E.S.G., V.K., D.K., M.S.B., B.T., L.K., M.B.; formal analysis: E.S.G., V.K., M.S., L.K., M.B.; investigation: E.S.G., V.K., D.K., M.S.B., M.S., L.K., M.B.; resources: L.K.; data curation: E.S.G.; writing—original draft: E.S.G., V.K., M.S.; writing—review & editing: E.S.G., V.K., D.K., T.L., B.T., L.K., M.B.; visualization: V.K.; supervision: E.S.G., B.T., L.K., M.B.; project administration: E.S.G., M.B.; funding: L.K. All authors have read and agreed to the published version of the manuscript.

Funding

V.K., K.D., M.S.B., T.L., L.K., M.B. acknowledges the support from microONE, a COMET Modul under the lead of CBmed GmbH, which is funded by the federal ministries BMK and BMDW, the provinces of Styria and Vienna, and managed by the Austrian Research Promotion Agency (FFG) within the COMET—Competence Centers for Excellent Technologies—program. V.K., K.D., M.S.B. and M.B. further acknowledge support by research subsidies granted by the government of Upper Austria (Grant Nr. FTI 2022 (HIQUA-MP): Wi-2021-303205/13-Au). L.K. also received support from the Austrian Federal Ministry of Science, Research and Economy, the National Foundation for Research, Technology and Development, and the Christian Doppler Research Association, as well as Siemens Healthineers for their financial and scientific support. L.K. was also supported by a European Union Horizon 2020 Marie Sklodowska-Curie Doctoral Network grants (FANTOM, n. P101072735 and eRaDicate, n. 101119427) the Christian-Doppler Lab for Applied Metabolomics (CDL-AM), and the Austrian Science Fund (grants FWF: P26011, P29251, P 34781

as well as the International PhD Program in Translational Oncology IPPTO 59.doc.funds). Additionally, this research was funded by the Vienna Science and Technology Fund (WWTF), grant number LS19-018. L.K. is a member of the European Research Initiative for ALK-Related Malignancies (www.erialcl.net).

Declarations

Competing interests

The authors declare no competing interests.

Additional information

Correspondence and requests for materials should be addressed to E.S.G., L.K. or M.B.

Reprints and permissions information is available at www.nature.com/reprints.

Publisher's note Springer Nature remains neutral with regard to jurisdictional claims in published maps and institutional affiliations.